The Effect of Particle Size and Volume Fraction on the Aging Behavior of a Liquid-Phase Sintered SiC/Aluminum Composite

G.M. JANOWSKI and B.J. PLETKA

The aging response of a SiC particulate reinforced powder metallurgy aluminum composite was examined as a function of particle size and volume fraction. The addition of SiC particles ranging in size from 24 to 142 μm at 9 vol pct had no effect on the aging kinetics of the composites. Acceleration of the aging behavior or inhibition of the initial stage of the age-hardening process was observed at 18 and 27 vol pct. The accelerated aging kinetics were consistent with smaller particles creating larger thermal misfit dislocation densities. In addition, it was shown that different combinations of ceramic particle size and volume fraction lead to similar effects on the aging behavior. Loss of the initial hardening response was attributed to the suppression of Guinier-Preston (GP) zone formation due to the annihilation of excess vacancies at the thermal misfit dislocations.

I. INTRODUCTION

IT has been well established that the addition of discontinuous ceramic particles or whiskers to aluminum matrices results in the composites exhibiting different aging kinetics compared to the unreinforced alloys. An acceleration in the aging kinetics of the composite materials has been frequently observed.[1–13] The accelerated aging was attributed to an increased dislocation density in the vicinity of the ceramic reinforcement, which hastens the nucleation and/or growth of the age-hardening precipitates. The increased dislocation density results from the differential thermal contraction between the particle and matrix produced on quenching the composite from the solutionizing step of the heat treatment (*e.g.*, Reference 14). However, it has also been shown that the initial stages of the precipitation sequence, *i.e.*, the formation of Guinier-Preston (GP) zones, can be suppressed by ceramic additions.[15] This alteration in the precipitation sequence is believed to result from a reduction in retained vacancies on quenching from the solutionizing temperature due to the annihilation of the vacancies, as has been discussed by Friend *et al.*[13]

Several models have been developed to estimate the dislocation generation due to thermal expansion mismatch.[16,17]Arsenault and Shi[16] have proposed a model in which prismatic punching of dislocations occurs in the vicinity of the ceramic reinforcement. From their analysis, the total dislocation density, ρ, due to prismatic punching can be written:

$$\rho = \frac{BV_f\varepsilon}{b\,(1 - V_f)}\,\frac{1}{t} \qquad [1]$$

where B is a geometric constant varying between 4 and 12 depending upon particle shape, V_f is the volume fraction of particles, ε is the misfit strain from the difference in thermal expansion coefficients, b is the magnitude of the Burgers vector, and t represents the smallest dimension of the particle. From Eq. [1], higher dislocation densities are predicted to result from smaller particle sizes and larger particle volume fractions. Equation [1] also suggests that different combinations of particle sizes and volume fractions can lead to the same dislocation density. Calculations of the particle volume fractions required to attain identical dislocation densities based on Eq. [1] are shown in Table I. It was assumed that the particles were spherical, and t in Eq. [1] was equated to the particle diameter. The calculations were performed for particle size (diameter) ratios of 2, 3, and 5. As the particle size ratio increases, greater volume fractions are required in order to achieve the same dislocation densities. While Eq. [1] calculates an overall dislocation density, the question of dislocation density as a function of distance from a ceramic particle was addressed both theoretically and experimentally by Kim *et al.*[17] They found that the dislocation densities were higher in the immediate vicinity of SiC particles and were indeed a function of ceramic particle size. Both of these models will be used to interpret the data of this study. The issue of age-hardening effects is much too complex to be addressed in a complete fashion using only these two models, but they are sufficient to explain to a first approximation the roles of particle size and particle volume fraction on the age-hardening behavior of aluminum alloy matrices.

The objective of the present work was to verify the dislocation generation model upon which Eq. [1] is based by examining the precipitation kinetics in a SiC-reinforced aluminum alloy in which the particle size and volume fraction were systematically varied. Particle sizes of 24, 63, and 142 μm were chosen so that a large particle size ratio (~6) was obtained between the largest and smallest particles while maintaining ratios of ~2.5 between the 24 and 63 μm particles and the 63 and 142 μm particles. The precipitation kinetics were monitored by determining the hardness as a function of aging time for the various composites. Selected composite and unreinforced alloy microstructures were ex-

G.M. JANOWSKI, formerly Graduate Student, Department of Metallurgical and Materials Engineering, Michigan Technological University, is Assistant Professor, Department of Materials Science and Engineering, University of Alabama at Birmingham, Birmingham, AL 35294-4461. B.J. PLETKA, Professor, is with the Department of Metallurgical and Materials Engineering, Michigan Technological University, Houghton, MI 49931.

Manuscript submitted January 31, 1991.

Table I. Particle Volume Percents Required for Identical Thermal Misfit Dislocation Densities as a Function of Particle Diameter Ratio

$V^*_{f_2}$ (Pct)	$V^*_{f_1}$ (Pct)		
	$(t_2^{**}/t_1) = 2$	$(t_2/t_1) = 3$	$(t_2/t_1) = 5$
5	2.6	1.7	1.0
10	5.6	3.6	2.2
20	11.1	7.7	4.8
30	17.7	12.5	7.9

*V_{f_1} and V_{f_2} = volume percent of particle diameters 1 and 2, respectively.

**t_1 and t_2 = diameters of particles 1 and 2, respectively.

amined using transmission electron microscopy (TEM) to assess the effect of the ceramic additions on the dislocation distributions and the age-hardening precipitates that were present.

II. PROCEDURE

The base alloy and composite materials were prepared by the press and sinter powder metallurgy method. In this technique, the desired elemental powders, 1.2 wt pct ACRAWAX* (a die wall lubricant), and ceramic particles were blended, compacted with a mechanical press at 142 MPa, sintered, and in this work, hot isostatically pressed (HIPped). Alloy 201 was selected as the base alloy and has a composition (in wt pct) of Al-4.4Cu-0.5 Mg-0.8 Si; the composition of alloy 201 is approximately equivalent to the cast and wrought alloy 2014. The SiC powders had average particle sizes of 24 (400 grit), 63 (240 grit), and 142 (120 grit) μm and were added to the Al-Cu-Si-Mg powder mixtures in amounts corresponding to 9, 18, or 27 vol pct of the fully dense matrix alloy. The particle size data were provided by the manufacturer; the particle size distributions are unimodal and are approximately a normal distribution. For example, the 63-μm mean particle size powder had 50 wt pct of the particles within ± 7 μm of the mean and 90 wt pct within ± 19 μm of the mean. The distributions are sufficiently narrow (and similar) that the three particle sizes used in the current study are significantly different.

*ACRAWAX is a trademark of Glyco, Inc., Norwalk, CT.

The sintering cycle consisted of degassing (400 °C ± 3 °C for 30 minutes) before sintering at 590 °C ± 3 °C for 1 hour; both of these steps were carried out in a nitrogen atmosphere. The samples were HIPped in argon at 510 °C and 142 MPa for a duration of 2 hours. The relative densities of the matrix alloy and 9 vol pct composite materials were greater than 99 pct of their theoretical values. The relative densities of the 18 vol pct and the 27 vol pct SiC composite materials were 95 to 97 pct and 93 to 96 pct, respectively. It should be noted that the decrease in density, associated primarily with clusters of SiC particles, leads to particle surface area which is not in intimate contact with the matrix. This loss of particle/matrix interface area would be expected to proportionally reduce the effect of the ceramic particles on age-hardening behavior. In addition, most of the comparisons of age-hardening curves will be done using materials of identical ceramic volume fractions and, therefore, similar densities.

The solutionizing and aging heat treatments were performed in air after HIPping and final specimen preparation. The solutionizing conditions were 510 °C ± 3 °C for 45 minutes, followed by a cold water quench. The specimens were then either aged immediately or stored at −20 °C for periods of less than 2 days; the aging temperature was 160 °C ± 3 °C, which is the standard heat-treatment temperature for a cast and wrought 2014 alloy. Samples to be aged for short time durations (≤4 hours) were solutionized and aged as a single batch to minimize inadvertent time and temperature variations. The range in aging times was 0.5 to 96 hours.

Ten Rockwell B hardness (HRB) measurements were made for each sample type and heat-treatment condition. Any datum which deviated from the average by more than 5 HRB was discarded; these low-reading data points were attributed to large subsurface pores. The remaining data were averaged and typically had a standard deviation of less than 1 HRB.

The microstructural development of selected specimens of the base alloy and the composite materials as a function of aging time was characterized with TEM. Specimens were prepared by sectioning, mechanical grinding, cutting disks, dimpling, and electropolishing. This sample preparation technique precluded the examination of the particle/matrix interface, since the ceramic phase does not electropolish under the same conditions as the aluminum alloy matrix. However, electropolishing offers the advantage (relative to ion milling) of not introducing ion damage or other sample preparation artifacts which may alter the original precipitation characteristics. Bright-field electron micrographs were taken under two-beam conditions using {111} reflections. The dislocations generated from the thermal expansion misfit were best observed after the disappearance of the helical dislocation loops (common in quenched aluminum alloys) and before the appearance of extensive precipitation.

III. RESULTS

A. *Matrix Alloy Microstructure and Aging Behavior*

The microstructure of the unreinforced matrix alloy is shown in Figure 1 and was found to consist of the aluminum matrix, large particles of the equilibrium form of the age-hardening precipitates (which remained undissolved during the solutionizing heat treatments), and constituent particles. The age-hardening precipitates and $MgAl_2O_4$ (spinel) were also observed when the microstructures were examined with TEM. The constituent phases, spinel, and particles of the equilibrium age-hardening phase, θ-$CuAl_2$, were located principally along the grain boundaries. The constituent phases were identified by electron diffraction as $(Fe,Cu)(Al,Cu)_6$, $CuMg_5Si_4Al_4$, $CuMg_4Al_6$, and Cu_2FeAl_7. A detailed description of the matrix alloy microstructure is given elsewhere.[18]

The HRB as a function of aging time for the alloy 201 matrix is shown in Figure 2. Alloy 201 follows the Al-Cu metastable precipitation sequence of GP zones $\rightarrow \theta'' \rightarrow \theta' \rightarrow \theta$. The large initial hardness increase is a result of GP zone formation; continued aging leads to the precipitation of the metastable θ''.[19] The hardness peak corresponds to the maximum volume fraction of θ'' and the approximate

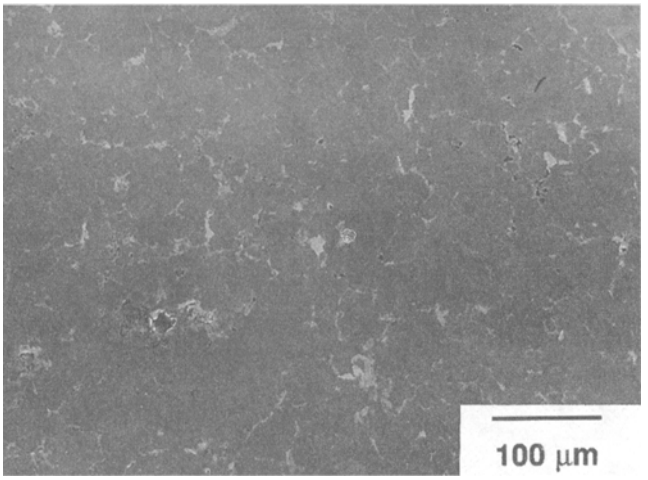

Fig. 1—Scanning electron micrograph of the unreinforced alloy 201 matrix.

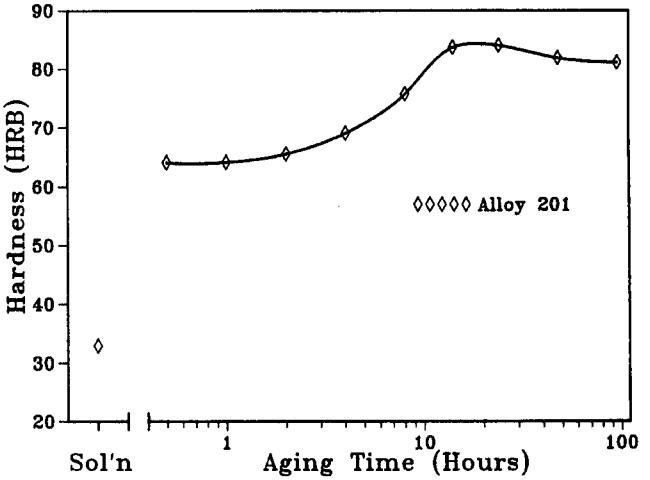

Fig. 2—HRB as a function of aging time for the unreinforced alloy 201 matrix.

beginning of metastable θ' precipitation. The general form of the aging curve and the time to peak hardness are consistent with data for cast and wrought alloys of similar composition.

Few dislocations were observed in the unreinforced matrix alloys; the majority of those present were located in the vicinity of constituent phases or other large particles. This observation is consistent with the work of Vogelsang *et al.* on unreinforced aluminum alloys.[14]

B. *Composite Material Microstructures*

Representative micrographs of the composites demonstrating some of the particle size and volume fraction combinations are given in Figure 3. No change in the matrix microstructure was observed when ceramic particles were added. The microconstituents which were found at the grain boundaries of the matrix alloys, spinel, and constituent phases were also present at the particle/matrix interfaces. In addition, the SiC interfaces were found to be partially faceted as a result of preferential attack of the particles by the liquid during sintering. Additional details of the interface microstructure and the mechanical properties of these composites have been presented elsewhere.[18]

A high, inhomogeneous dislocation density was found in the SiC-reinforced composites; examples of areas with high and low dislocation densities within the same specimen are shown in Figures 4(a) and (b), respectively. This composite, reinforced with 9 vol pct of 142 μm particles, would be expected to have the lowest misfit dislocation density based upon Eq. [1]. A representative electron micrograph of an area midway between 63 μm particles in a 9 vol pct composite is shown in Figure 4(c). A higher dislocation density is present than in Figure 4(b), as expected. These results are consistent with the theoretical and experimental work of Kim *et al.*[17] and the *in situ* observations of Vogelsang *et al.*[14]

C. *Composite Materials Aging Behavior*

The HRB of the 9 vol pct composites as a function of aging time at 160 °C are shown in Figure 5. It is apparent that the addition of a low volume fraction of SiC in the size range of 24 to 142 μm does not alter the aging behavior. Indeed, the hardness data for these three composites and the matrix alloy can be reasonably placed on the same aging curve. These results are consistent with the model in which dislocations are introduced into the matrix by virtue of the difference in thermal expansion coefficients. That is, the addition of 9 vol pct SiC particulate in the size range of 24 to 142 μm generates an insufficient amount of thermal expansion misfit dislocations to affect the age-hardening behavior of alloy 201.

The addition of 18 vol pct SiC particles results in changes in the aging behavior of alloy 201; the form that the changes take is a function of ceramic particle size, as shown in Figure 6. The addition of the 63 μm SiC particles was found to accelerate the aging response of the alloy; *i.e.*, the peak hardness occurred after 4 hours of aging rather than the 14 hours required by the matrix alloy (Figure 6). This result is nearly identical to the observations of other workers such as Christman and Suresh in their study of 2124 reinforced with 13 vol pct SiC whiskers[4] and Dutta and Bourell who reinforced 6061 with 10 vol pct SiC whiskers.[6] In contrast, the initial aging response of the composite reinforced with 24 μm particles was retarded since the large increase in hardness that occurred in the unreinforced matrix between the solutionized condition and 0.5 hours of aging was not observed. Further aging of the 24 μm SiC-reinforced composites resulted in a gradual increase in hardness with a peak taking place at approximately 14 hours. The aging behavior of the 142 μm composites is not clearly defined, although the data appear to roughly follow the aging response of the matrix. The large interparticle spacings that arise from an addition of 18 vol pct of 142 μm particles likely led to a very inhomogeneous distribution of dislocations (*i.e.*, primarily in the vicinity of the SiC particles) as well as a lower overall dislocation density, since large particles (at constant volume fraction) are expected to produce fewer dislocations according to Eq. [1]. Inhomogeneous dislocation densities were observed in the 9 vol pct 142 μm composites (Figures 4(a) and (b)), although the degree of the inhomogeneity may be reduced due to overlapping of the dislocation fields from neighboring particles in the 18 vol pct composite. What is important to recognize is that three distinct aging

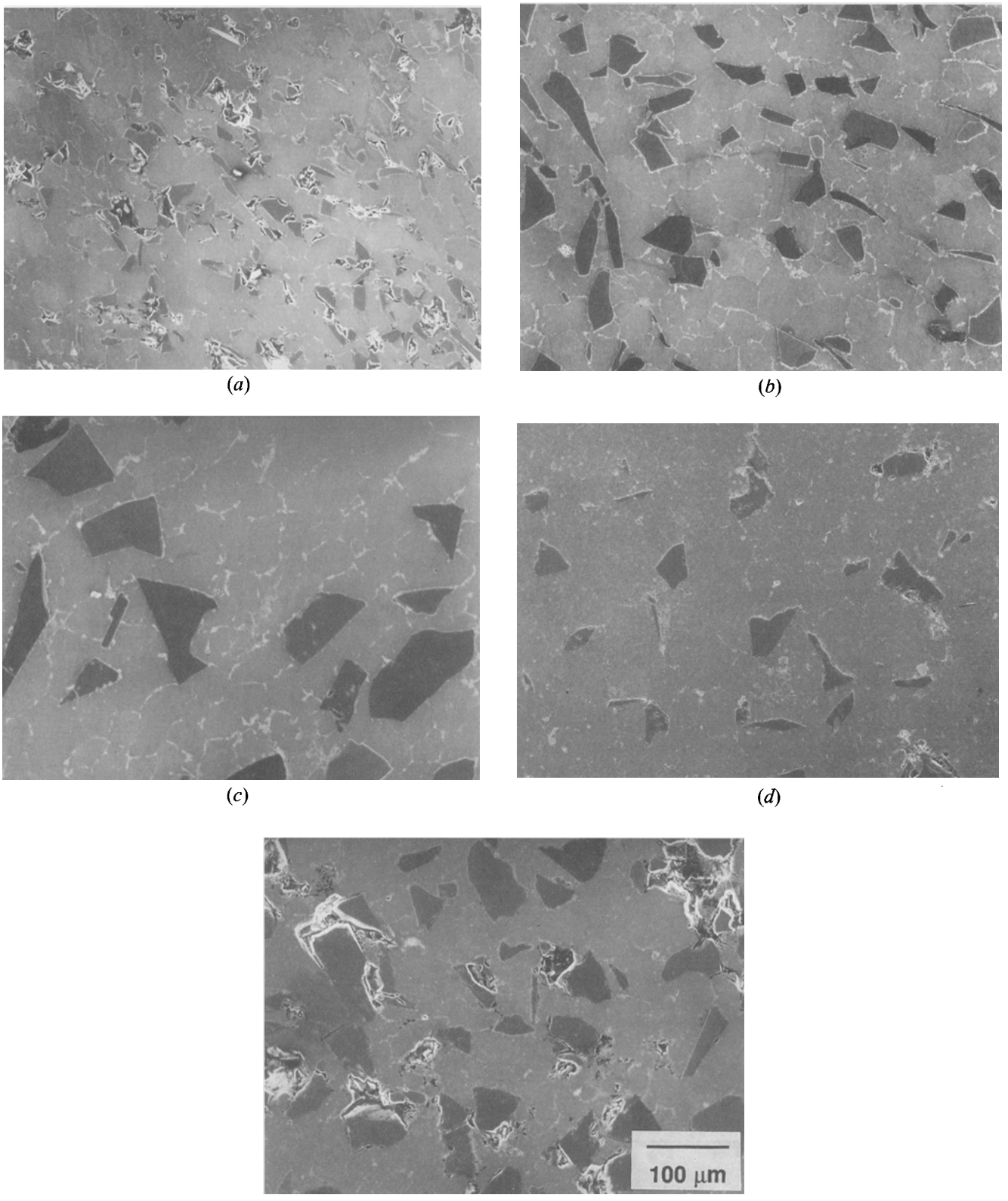

Fig. 3—Scanning electron micrographs of representative alloy 201-based composites reinforced with 18 vol pct: (*a*) 24 μm SiC, (*b*) 63 μm SiC, (*c*) 142 μm SiC, as well as (*d*) 9 vol pct and (*e*) 27 vol pct 63 μm SiC.

behaviors were observed in the 18 vol pct reinforced composites.

The microstructures of the alloy 201 matrix and the 18 vol pct 63 μm SiC-reinforced composite are nearly indistinguishable after 14 hours of aging at 160 °C, as can be seen by comparing Figures 7(a) and (b). However, a comparison of these two materials after 4 hours of aging demonstrates the accelerated aging of the SiC-reinforced

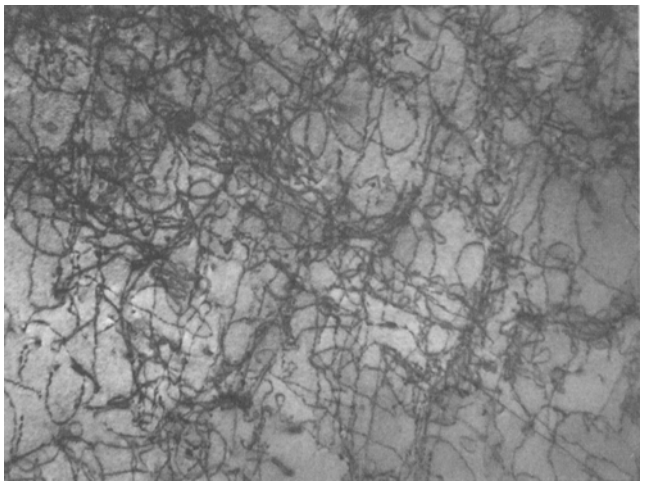

(*a*)

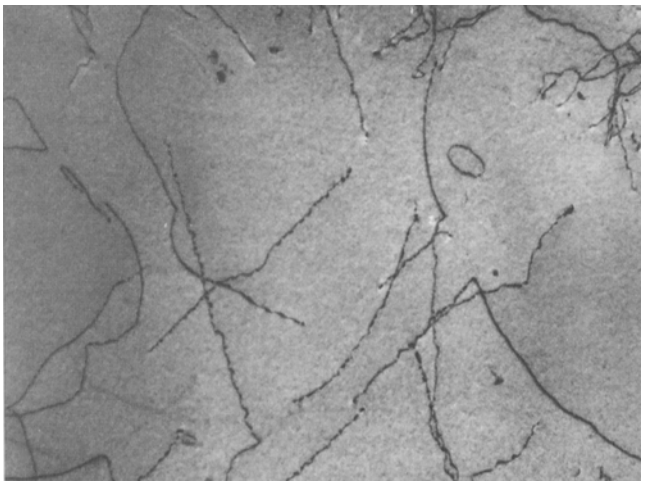

(*b*)

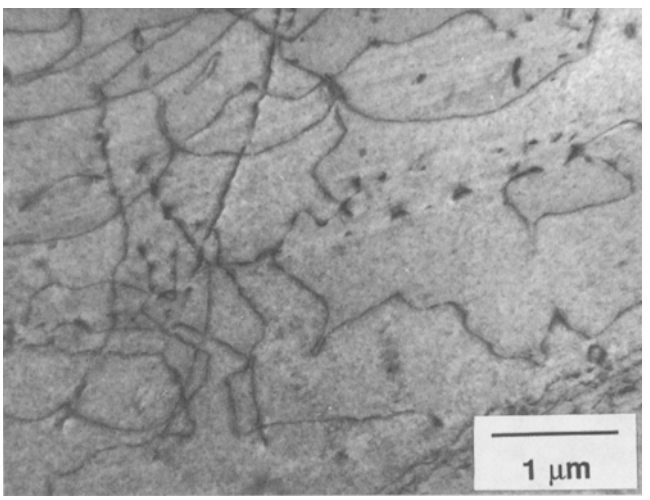

(*c*)

Fig. 4—Transmission electron micrographs of the 9 vol pct, 142 μm SiC composite illustrating the (*a*) high dislocation densities present near the SiC particles and (*b*) lower dislocation densities present in areas between particles. Higher dislocation densities occur midway between particles in composites reinforced with (*c*) 9 vol pct 63 μm SiC. All micrographs were taken with {111} two-beam conditions resulting in one-half of the *a*/2⟨110⟩ dislocations being invisible.

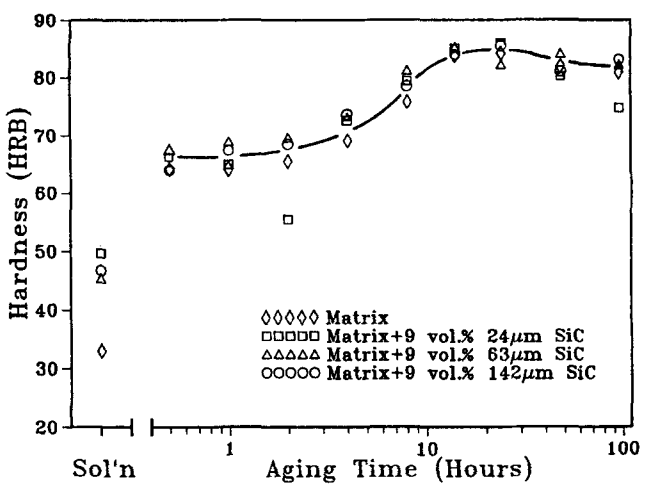

Fig. 5—HRB as a function of aging time at 160 °C for the 9 vol pct composite materials.

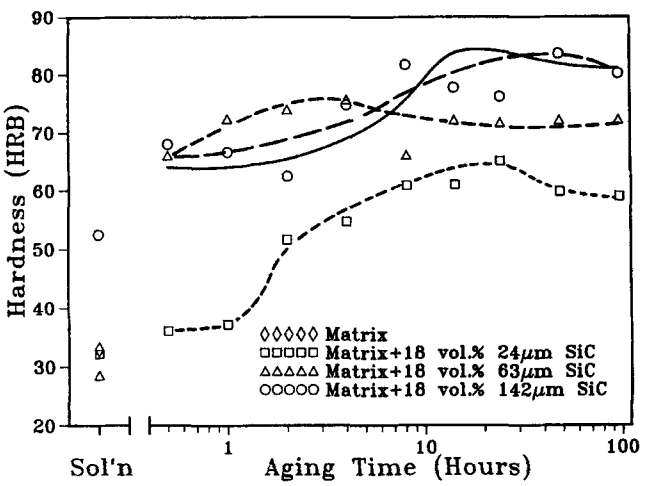

Fig. 6—HRB as a function of aging time at 160 °C for the 18 vol pct composite materials. The solid dark line is the aging curve for the unreinforced matrix (without data points).

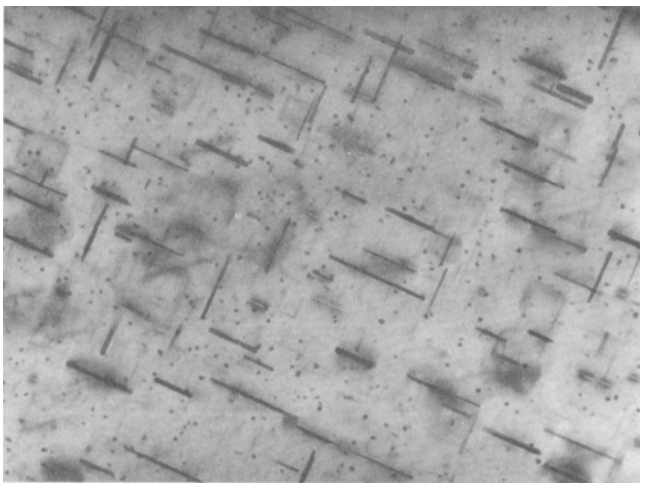

(*a*)

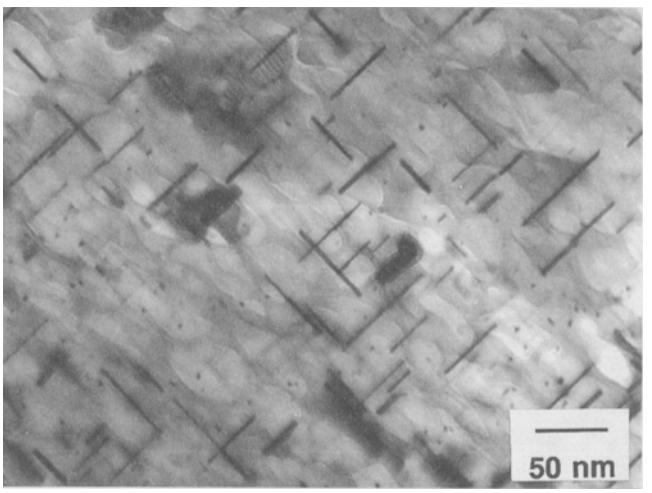

(*b*)

Fig. 7—Transmission electron micrographs of the microstructures of the (*a*) unreinforced matrix alloy and (*b*) 18 vol pct 63 μm SiC composite after 14 hours of aging at 160 °C.

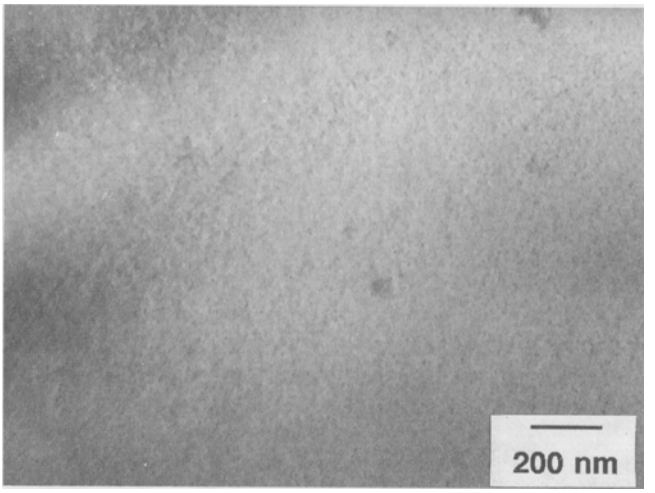

(*a*)

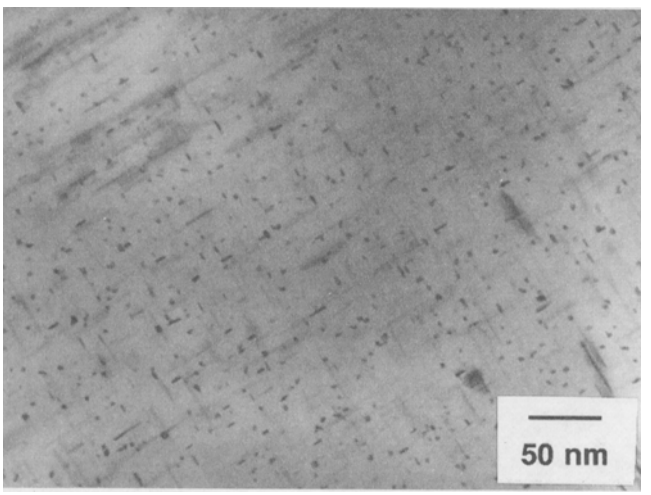

(*b*)

Fig. 8—Transmission electron micrographs of the microstructures of the (*a*) unreinforced matrix alloy and (*b*) 18 vol pct 63 μm SiC composite after 4 hours of aging at 160 °C.

composite. The matrix alloy is generally featureless when examined with TEM (Figure 8(a)). The lack of visible precipitation and the hardness increase indicate that GP zones are present but are not visible in this micrograph. However, the composite material contains extensive amounts of θ'' precipitation and, likely, GP zones after 4 hours of aging. This precipitation is shown in Figure 8(b) with a bright-field micrograph of a foil oriented near the [001] zone axis where the precipitate contrast of one of the three θ'' variants is maximized and the dislocations are not visible. (Under most imaging conditions, the combined contrast from the precipitates and the many dislocations makes it impossible to discern any features individually.) The precipitate microstructure observed in Figure 8(b) is typical of the unreinforced matrix when aged to peak hardness. It can, therefore, be concluded that the accelerated aging of this composite is a result of earlier nucleation of θ''.

The hardness data as a function of aging time for the composites with 27 vol pct SiC are plotted in Figure 9. The aging behavior of all three composites is approximately the same and a single curve has been drawn through the data

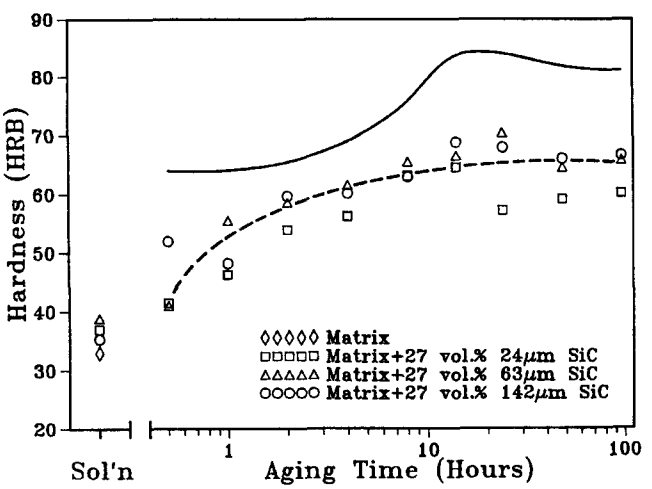

Fig. 9—HRB as a function of aging time at 160 °C for the 27 vol pct SiC composite materials. Note the lack of a substantial hardness increase after 0.5 hours of aging for all particle size composites.

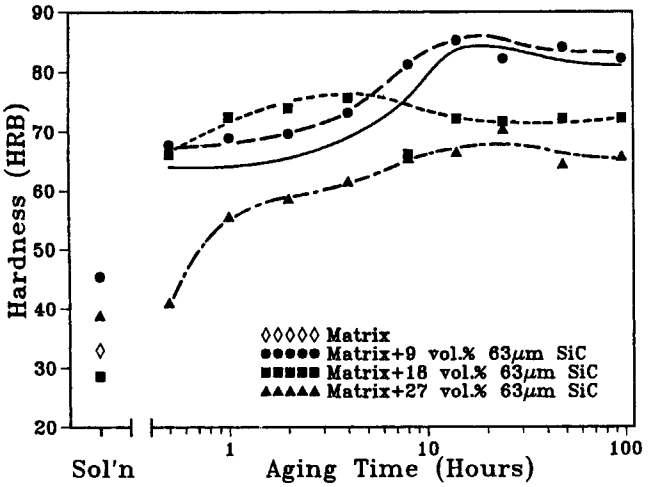

Fig. 10—HRB as a function of aging time at 160 °C for the alloy 201-based composite materials reinforced with 9, 18, and 27 vol pct 63 μm SiC.

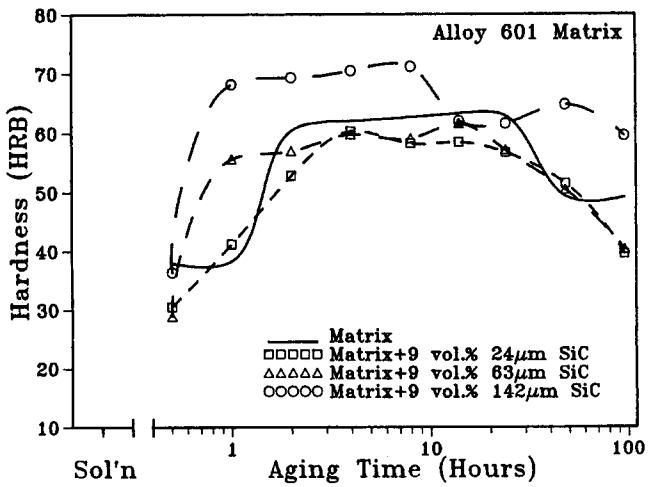

Fig. 11—HRB as a function of aging time at 175 °C for the alloy 601-based, 9 vol pct ceramic composite materials.

Table II. Thermal Misfit Dislocation Densities Calculated Using Equation [1] ($\times 10^{-8}$ cm/cm^3)

Particle (Vol Pct)	Particle Size (μm)		
	24	63	142
9	1.7	0.63	0.28
18	3.7	1.4	0.62
27	6.2	2.4	1.1

points. A gradual increase in hardness after 0.5 hours of aging was found with a fairly constant hardness after approximately 8 hours at 160 °C. This curve is very similar to the behavior of the 18 vol pct 24 μm SiC-reinforced composites. Thus, as the volume fraction of the larger sized particles increases, these composites mimic the behavior of the smaller size particle composites as the dislocation density within the matrix microstructure increases.

An overall view of the effect that varying the ceramic volume fraction has on the aging response is shown in Figure 10, where the data for the composites reinforced with 9, 18, and 27 vol pct 63 μm SiC are shown. The 9 vol pct composite exhibited the same hardness curve as the matrix alloy, the 18 vol pct composite showed accelerated aging, and the 27 vol pct composite did not show the large initial hardness increase typical of the alloy 201 matrix. This figure indicates that the full range of aging effects can be observed with a single particle size.

IV. DISCUSSION

The hardness data for the 9 vol pct composites showed that an insufficient quantity of dislocations was introduced into the matrix (in the range of particle sizes considered) to measurably affect the aging kinetics. This result demonstrates that a critical ceramic volume fraction exists below which the aging behavior is unaltered. This critical volume fraction is a function of particle type (composition and, likely, morphology), particle size, and matrix composition. Previous investigations which have examined the aging kinetics of aluminum matrix composite materials did not indicate such a critical volume fraction exists. However, these studies used much smaller particle sizes, typically SiC whiskers with a diameter of 0.5 μm (*e.g.*, References 4 and 6). The thermal misfit dislocation density would be higher in these composites, since $\rho \propto 1/t$ from Eq. [1], and apparently of sufficient magnitude to affect the aging kinetics.

The critical volume fraction necessary to affect the age-hardening behavior would also be expected to be a function of the precipitation sequence and, therefore, the alloy composition. This hypothesis was tested by examining the aging kinetics of alloy 601 (which is approximately equivalent in composition to the cast and wrought aluminum alloy 6061 and is strengthened by the Al-Mg-Si metastable phase series) reinforced with 9 vol pct SiC particles of the same sizes used in the 201 alloy composites. It is evident in Figure 11 that the time to peak hardness is accelerated by the addition of all sizes of SiC, except, possibly, the 24 μm particles. It can, therefore, be concluded that the critical volume fraction is between 9 and 18 vol pct SiC in alloy 201 and less than 9 vol pct SiC in alloy 601. However, it is important to recognize that the critical volume fraction is a function of particle size; a smaller particle size will reduce the critical ceramic volume fraction for a given alloy. Thus, the aging responses at low volume fractions observed with other matrix alloys[4,6] may also be due to the different matrix alloys as well as the smaller particle sizes (discussed previously).

Once the critical volume fraction is exceeded, the aging kinetics are expected to depend on particle size since small particles generate more dislocations than do large particles (Eq. [1]). The data of this study are consistent with this model, because the aging behavior of the 24 μm SiC composites at a given volume fraction is often repeated for the larger particle sizes at the next higher volume fraction. These results can be interpreted by considering the role of dislocations in precipitate nucleation in aluminum alloys. It is well known that dislocations act as heterogeneous nucleation sites;[20–23] this results in shorter times to attain the peak-aged condition and, in some cases, a higher peak strength. For example, the nucleation of θ'' was demonstrated to occur at earlier aging times when 18 vol pct 63 μm SiC was added to alloy 201. Dislocation densities were calculated using Eq. [1] and are shown in Table II as a function of particle size and volume fraction for the com-

posites of this study. The misfit strain was calculated using the difference between the solutionizing temperature and room temperature for ΔT. This approach overestimates ΔT, since a certain stress must be exceeded before plastic deformation would begin in the matrix and plastic relaxation of the stress would occur at higher temperatures. Nonetheless, the relative values are informative. For example, examination of Table II indicates the dislocation density of the 27 vol pct 142 μm SiC-reinforced composite never exceeds the value for the 9 vol pct 24 μm SiC composite, yet alterations in the aging kinetics for the former were observed. Also, the changes in dislocation density with increasing volume fraction of SiC for each increment in particle size are less than an order of magnitude, but significant changes in aging kinetics were observed for each particle size. These observations suggest that additional factors must be taken into consideration before a fully quantitative model is possible, including refinement of the dislocation density models and/or inclusion of the inhomogeneous nature of the dislocation distribution.

The lack of a hardness increase after 0.5 hours of aging in the higher volume fraction/smaller particle size composites cannot be attributed to dislocation enhanced precipitation kinetics. Rather, a mechanism which slowed down or eliminated a step in the aging sequence must now be operative. The calorimetry results of Papazian[15] indicated that SiC additions reduced the quantity of GP zones in all of the Al alloys that he studied; it was hypothesized that the dislocations acted as vacancy annihilation sites. Ceresara and Fiorini[24,25] also showed that the presence of 1 to 3 wt pct finely dispersed submicron oxides prevented the formation of GP zones in air-milled alloy 201 and alloy 601 due to a loss of excess vacancies. Thus, previous results as well as those of the present study indicate that the addition of ceramic particles can reduce the quantity of excess vacancies and, in the limiting case, eliminate the initial stage of age hardening. It should also be pointed out that accelerated aging kinetics (through dislocations) and vacancy annihilation are not independent since the removal of GP zones may affect the remaining steps of the aging sequence.

The aging curves indicate that the particle size dependency is lost at high volume fractions (*i.e.*, 27 vol pct) as the effects of dislocations on aging reach a "saturation" level. In other words, the continued increase in dislocation density with increasing volume fraction (or decreasing particle size) no longer alters the aging kinetics, since nucleation is no longer the rate limiting step in the nucleation and growth process of the precipitates. For example, diffusion of the solute(s) may become the rate controlling step in the precipitation process as the number of nucleation sites exceeds some critical value (ignoring dislocation pipe diffusion).

V. CONCLUSIONS

1. A critical ceramic volume fraction, which is a function of the particle size and age-hardening precipitation sequence (and, therefore, alloy composition), must be exceeded in order to affect the aging behavior.

2. Small particle sizes and high volume fractions were more effective in altering the aging behavior of composites based on alloy 201, consistent with the model Arsenault and Shi[16] used to develop Eq. [1] in which the generation of thermal misfit dislocations occurs from the differences in thermal expansion of SiC and the Al matrix.

3. Accelerated aging occurs when the critical volume fraction is exceeded. Further ceramic additions led to a loss of the initial hardening due to the suppression of GP zone formation. The latter result was attributed to the loss of excess vacancies at the thermal misfit dislocations.

4. The diversity of the observed effects of ceramics additions on the aging behavior of composites in this study can be interpreted to a first approximation by considering the role that thermal misfit dislocations have in the precipitate nucleation kinetics in aluminum alloys and the fact that various combinations of ceramic size and volume fraction can produce equivalent effects upon aging in a particular alloy.

ACKNOWLEDGMENTS

The primary support for this research was furnished by Alcoa; the authors wish to thank various Alcoa personnel, particularly Warren H. Hunt, Jr., for their guidance and suggestions through this project. Additional support for GMJ was given in the form of a fellowship by the Graduate School, Michigan Technological University, and from the NSF-EPSCoR program Composite Materials: Tailored Interfaces while at the University of Alabama at Birmingham.

REFERENCES

1. T.G. Nieh and R.F. Karlak: *Scripta Metall.*, 1984, vol. 18, pp. 25-28.
2. K.K. Chawla and M. Metzger: *J. Mater. Sci.*, 1972, vol. 7, pp. 34-39.
3. R.J. Arsenault and R.M. Fisher: *Scripta Metall.*, 1983, vol. 17, pp. 67-71.
4. T. Christman and S. Suresh: *Acta Metall.*, 1988, vol. 36, pp. 1691-1704.
5. T. Christman, A. Needleman, S. Nutt, and S. Suresh: *Mater. Sci. Eng.*, 1989, vol. A107, pp. 49-61.
6. I. Dutta and D.L. Bourell: *Mater. Sci. Eng.*, 1989, vol. A112, pp. 67-77.
7. Ram B. Bhagat, Maurice F. Amateau, Michael B. House, Kenneth C. Meinert, and Paul Nisson: *J. Comp. Mater.*, 1992, vol. 26, pp. 1578-93.
8. R.U. Vaidya, Z.R. Xu, X. Li, K.K. Chawla, and A.K. Zurek: *J. Mater. Sci.*, 1994, vol. 29, pp. 2944-50.
9. Michael B. House, Kenneth C. Meinert, and Ram B. Bhagat: *JOM*, 1991, vol. 43, pp. 24-28.
10. M.J. Hadianfard, Yiu-Wing Mai, and J.C. Healy: *J. Mater. Sci.*, 1993, vol. 28, pp. 3665-69.
11. Y. Song and T.N. Baker: *Mater. Sci. Technol.*, 1994, vol. 10, pp. 406-13.
12. M.P. Thomas and J.E. King: *J. Mater. Sci.*, 1994, vol. 29, pp. 5272-78.
13. C.M. Friend, I. Horsfall, S.D. Luxton, and R.J. Young: in *Advances in Cast Metal Matrix Composites*, S.G. Fishman and A.K. Dhingra, eds., ASM INTERNATIONAL, Metals Park, OH, 1988, pp. 309-15.
14. M. Vogelsang, R.J. Arsenault, and R.M. Fisher: *Metall. Trans. A*, 1986, vol. 17A, pp. 379-89.
15. J.M. Papazian: *Metall. Trans. A*, 1988, vol. 19A, pp. 2945-53.
16. R.J. Arsenault and N. Shi: *Mater. Sci. Eng.*, 1986, vol. 81, pp. 175-87.
17. C.T. Kim, J.K. Lee, and M.R. Plichta: *Metall. Trans. A*, 1990, vol. 21A, pp. 673-82.
18. G.M. Janowski and B.J. Pletka: *Mater. Sci. Eng.*, 1990, vol. A129, pp. 65-76.
19. J.T. Staley, R.F. Ashton, I. Broverman, and P.R. Sperry: in *Aluminum: Properties and Physical Metallurgy*, John E. Hatch, ed., ASM, Metals Park, OH, 1984, pp. 134-99.

20. J.W. Cahn: *Acta Metall.*, 1957, vol. 5, pp. 169-72.
21. F.S. Ham: *J. Appl. Phys.*, 1959, vol. 30, pp. 915-26.
22. S. Harper: *Phys. Rev.*, 1951, vol. 83, pp. 709-12.
23. A.H. Cottrell and B.A. Bilby: *Proc. Phys. Soc., London, Sect. A*, 1949, vol. 62, pp. 49-62.
24. S. Ceresara and P. Fiorini: *Powder Metall.*, 1979, vol. 22, pp. 1-4.
25. S. Ceresara and P. Fiorini: *Powder Metall.*, 1981, vol. 24, pp. 210-13.